Photometric Capabilities and Scientific Applications of the Meshtitsa Private Observatory

Nikola Antonov[1]
Institute for Advanced Physical Studies, 111 Tsarigradsko Shose Boulevard, Sofia, Bulgaria, and Department of Astronomy, Faculty of Physics, Sofia University, 5 James Bourchier Boulevard, Sofia, Bulgaria; nikola.antonov@iaps.institute

Received December 19, 2025; revised January 9, 2026; accepted January 9, 2026

Abstract This paper presents the Meshtitsa Observatory—a small-aperture technical platform for high-precision photometric astronomical observations. Located near Pernik, Bulgaria, it is a privately operated roll-off-roof facility equipped with a 0.25-m telescope, CMOS camera, and photometric filters. All operations are remotely managed using a Debian-based INDIGO server infrastructure. The observatory has successfully captured light curves of cataclysmic stars, stellar flares, and transit events of hot Jupiter-type exoplanets with sufficient photometric precision for scientific analysis. These results demonstrate the viability of small-aperture observatories.

1. Introduction

Within professional optical astronomy, telescopes are commonly sorted by aperture into *small* (D ≤ 2 m), *medium* (2–5 m), and *large* (6–12 m) categories (NRC 2015). In the non-professional realm, the threshold shifts downward; the NASA's Exoplanet Watch program, for example, designates any instrument with D ≤ 1 m as "small" and shows that telescopes as modest as 0.15–0.25 m routinely supply transit ephemerides and high-cadence light curves of variable targets (Zellem *et al.* 2020). Because they are affordable, easily automated, and rapidly re-tasked, small telescopes remain indispensable for tracking swiftly evolving phenomena, ranging from near-Earth asteroids and cataclysmic variable stars to shallow exoplanet transits, and they often provide the first layer of discovery and follow-up, leaving larger telescopes free for deep imaging and high-resolution spectroscopy.

Cataclysmic variables (CVs) are a group of stars that show sudden and unpredictable changes in brightness. Nowadays, it is well known that their high-amplitude outbursts are due to an increased accretion rate onto the disk formed around the more massive companion of a close binary system, comprised of a white dwarf and a late-type main-sequence star. Their erratic behavior has attracted both professional and non-professional astronomers. Even small telescopes make them visible, and hundreds more can be monitored using modern CCD/CMOS cameras. The field is especially open to community contributions, as professionals cannot monitor all known objects.

The study of distant planets has also become a field of activity for both professional and citizen scientists. Several indirect methods for exoplanet research and discovery have been utilized, most notably the transit method, which is available for small-aperture ground-based observations—a telescope with an aperture of 0.25 m can achieve accurate enough results to obtain a good model fit, e.g. Fowler *et al.* (2021).

Stellar flares are high-energy events on stellar surfaces, triggered by the reconnection of magnetic field lines. They are believed to occur in the upper atmosphere of all main-sequence stars that possess a convective layer and are driven by similar physical processes. In the Sun, flares arise in regions of enhanced magnetic activity, whereas in M-dwarf stars, these events seem to occur across the whole stellar surface (Benz and Güdel 2010).

In this study, we present results from observations of CV stars—a newly discovered dwarf-nova superhumps during superoutburst, exoplanet transit, and stellar flares of an M-dwarf star conducted at the Meshtitsa Observatory, indicating sufficient photometric precision of small astronomical telescopes, operated entirely remotely and in an automated manner. The Meshtitsa Observatory is a private, donation-funded astronomical facility featuring a typical roll-off-roof design, optimized for remote management. Located in the village of Meshtitsa, near Pernik, Bulgaria, the site sits at an altitude of 690–695 m at coordinates: 42.67° N, 23.00° E.

The observatory operates under Bortle class 4 skies, providing favorable conditions for astronomical observations. With an average of ≈200 clear nights per year, the facility is dedicated to continuous time-domain monitoring using a small-aperture telescope.

2. System configuration

2.1. Telescope

The observatory is equipped with a Sky-Watcher Telescope N 250 / 1200 PDS Explorer BD OTA[2], shown in Figure 1. The telescope is fitted with a Baader MPCC Mark III coma corrector. The optical parameters of the system are shown in Table 1.

Table 1. Sky-Watcher Telescope N 250/1200 PDS Explorer parameters.

Parameter	*Value*
Optical design	Parabolic Newtonian reflector
Aperture (mm)	250
Focal length (mm)	1200
Aperture ratio (f/)	4.8
Tube length (mm)	1120
Tube weight (kg)	14.5

[1] https://orcid.org/0009-0002-1484-7029

Although operating near the limits of its load capacity, the German equatorial mount EQ6-R Pro[3] provides reliable object tracking. Automatic guiding is achieved using a TS Optics Guidescope AC 80/600[4] with an ASI290MC guiding camera[5]. The guiding process is controlled by the INDIGO software framework, which supports a variety of guiding algorithms to ensure stable tracking and high-quality guiding performance during long exposure sequences. The system is optimized to deliver an average RMSE guiding error below 0.5".

The entire system is managed by the INDIGO platform and the Ain INDIGO Imager running on a Linux operating system, which is also being used at professional observatories[6]. The INDIGO software enables full remote control and an automated workflow, including pointing, highly detailed task scheduling for exact times, roof opening and closing, and sky-condition monitoring in cooperation with a CloudWatcher[7] device (cloud cover monitoring, precipitation, and alarms when unfavorable weather conditions arise). With this integrated software-and-hardware setup, the observatory operates completely autonomously, eliminating the need for constant supervision during observations.

2.2. Filters

The telescope at the Meshtitsa Observatory is equipped with a photometric Baader UBVR Bessel Filter Set 36 mm[8] (Figure 2).

Following best practices and the recommendations outlined in the *AAVSO Guide to CCD/CMOS Photometry*, Chapter 6 (AAVSO 2022), tests were conducted to improve photometric accuracy by imaging standard fields to measure transformation coefficients for each filter. The coefficients shown in Table 2 are derived using the AAVSO Transform Generator (AAVSO 2014).

2.3. Camera

The ASI 533 MM Pro[9] camera is a high-performance monochrome imaging device well-suited for both artistic astrophotography and scientific research (see Figure 3). It features a Sony IMX533 back-illuminated CMOS sensor. One of its major advantages is the complete absence of amp glow, which results in exceptionally clean raw images and simplifies the calibration process.

The ASI 533 MM Pro also has a dual-stage TEC cooling system that can reduce the sensor temperature by up to 35° C below ambient, effectively minimizing thermal noise during long exposures. The camera parameters are summarized in Table 3.

The sensor quantum efficiency curve (QE), shown in Figure 4 peaks above 90% in the blue-green part of the spectrum (approximately 450–500 nm), making it highly efficient for most photometric work in the B, V, and R bands. ASI 533 MM Pro has limited sensitivity in the U band, with quantum efficiency dropping significantly around 350–400 nm. Although U-band photometry can be performed with this camera, it requires considerably longer exposures than in the B- or V-band.

A linearity test was conducted under stable observational conditions. The ASI533MM Pro camera was operated at a constant sensor temperature of 0° C , using a steady, uniformly

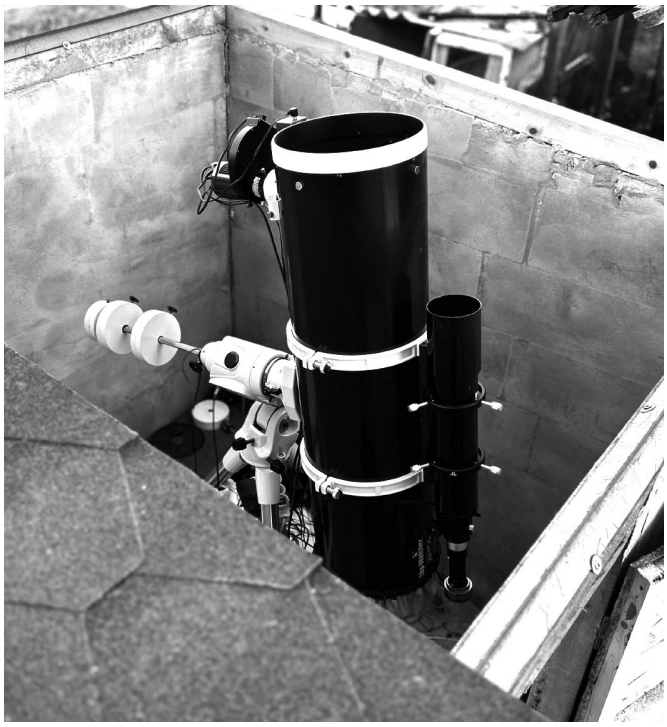

Figure 1. The telescope at the Meshtitsa Observatory, a 0.25m Sky-Watcher Newtonian reflector (f/4.8, focal length 1200mm) mounted on an EQ6-R Pro German equatorial mount.

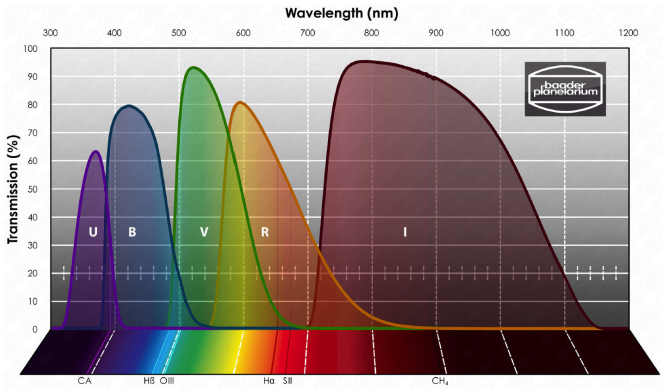

Figure 2. Spectral profile of Baader Bessel-UBVRI Filters. Image source: Baader Planetarium (2026).

Table 2. Standard-system transformation coefficients derived for the Meshtitsa telescope.

Coefficient	*Value*	*Error*
T_{bv}	1.095	0.009
T_{b_bv}	0.080	0.012
T_{br}	1.144	0.013
T_{b_br}	0.050	0.006
T_{v_bv}	–0.008	0.015
T_{vr}	1.255	0.033
T_{v_vr}	–0.012	0.025
T_{r_vr}	–0.221	0.030

Figure 3. Camera ASI533 MM Pro CMOS, filter wheel, and automatic focuser mounted on the 0.25-m telescope.

Table 3. ASI 533 MM Pro camera parameters.[1]

Parameter	*Value*
Sensor	CMOS Chip (Sony IMX533)
Light spectrum	U (limited sensitivity) + Visible + NIR
Total pixels	9 MP
Resolution W x H	3 008 × 3 008 px
Pixel size	3.76 µm
Bit depth	14
Full well capacity	50 000
Max. cooling difference below ambient temperature	35° C
Weight	410 g

[1] *Source: https://www.zwoastro.com/product/asi533-pro-series/*

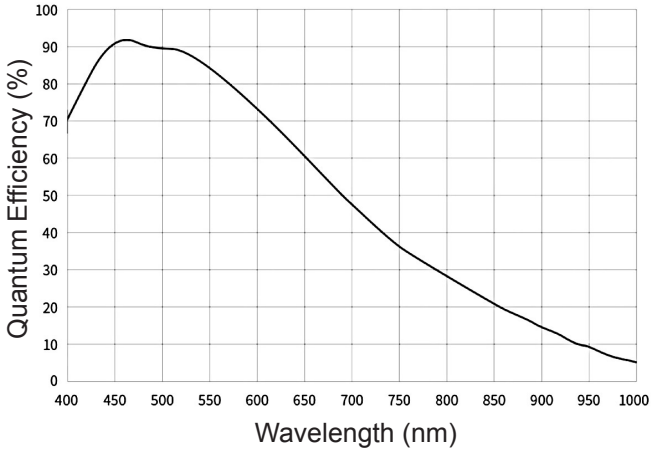

Figure 4. Quantum Efficiency of ASI533MM Pro CMOS camera according to the manufacturer's website. Image source: Suzhou ZWO Co., Ltd. (2026).

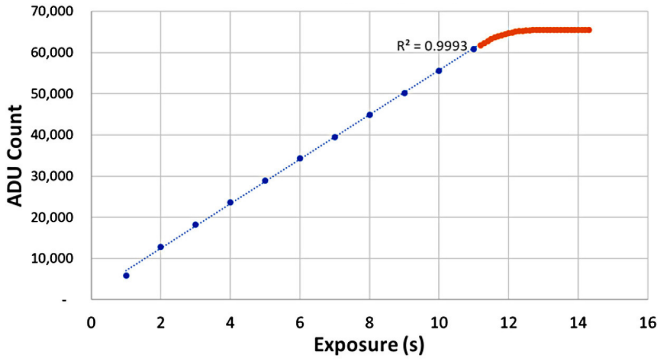

Figure 5. Linearity test (Gain 0, Offset 10) for the ASI533MM camera in Meshtitsa Observatory showing relation between ADU counts and exposure time.

illuminated surface as the light source. A broadband L (luminance) filter was placed in the optical path. Exposure times were varied from 1.0 to 15.0 seconds in steps of 1.0 second, and the camera settings were fixed at Gain = 0 and Offset = 10 to maximize dynamic range. For each exposure, the mean ADU value for the frame was measured.

The resulting data, shown in Figure 5, demonstrate a well-defined linear response up to approximately 60,000 ADU. Beyond this level, the response begins to flatten as the detector approaches its saturation regime. Although the sensor uses a 14-bit analog-to-digital converter (ADC), its output is internally mapped to a 16-bit format, allowing for digital values up to 65,535. The maximum recorded value in fully saturated pixels is 65,532 ADU. For optimal photometric results, exposures should be adjusted to keep the peak signal below ~60,000 ADU, thereby avoiding non-linear compression near the ADC ceiling.

2.4. Optical performance

The Meshtitsa Observatory is located near Pernik, Bulgaria, at an altitude of 695 m. The typical seeing conditions are characterized by FWHM between 2.0"and 2.5". Under a clear, moonless night, and with the telescope pointed at an altitude of at least 60° above the horizon, the current optical system achieves a limiting magnitude of ≈17.5 in the V band with a 30-second exposure at a signal-to-noise ratio of ≈7, which was estimated by the astrometric software ASTAP[10]. Long-term measurements performed over several months with a Lunatico Astronomia CloudWatcher[11] indicate that the maximum sky darkness at the site reaches 19.7 mag/arcsec^2.

For a system with 3.76 µm pixel size and 1200 mm focal length, a scale of 0.64" per pixel is close to oversampling for typical seeing conditions at a given location. At 2 × 2 binning, the resulting pixel scale is approximately 1.3" per pixel, which better matches the atmospheric resolution limit. At a focal length of 1200 mm, combined with the sensor size of 11.31 × 11.31 mm, the system provides a field of view of approximately 0.5° × 0.5°.

As an example, Figure 6 shows a V425 Cas stellar field from a 300-second calibrated science image.

The image generated by the ASTAP aberration inspector (Figure 7) displays star cutouts sampled from a 3 × 3 grid, demonstrating how the PSF varies across the field.

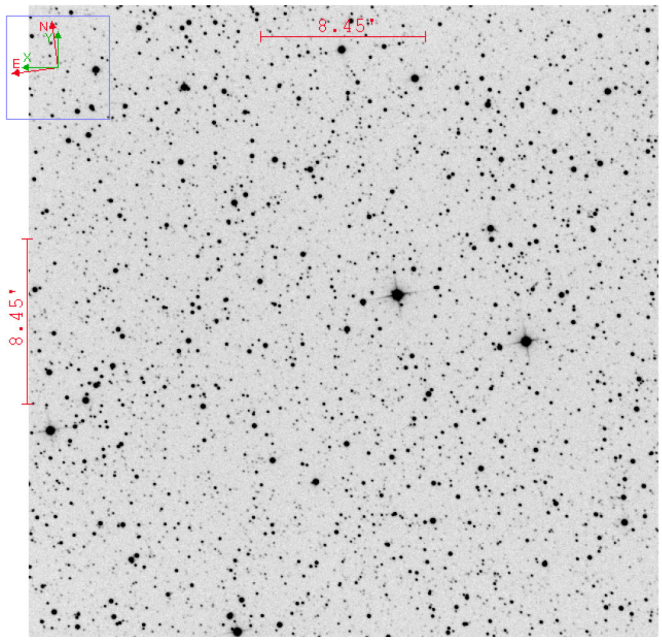

Figure 6. Single calibrated frame of a V425 Cas stellar field obtained with the V filter (300 s exposure, 2 × 2 binning, gain 0, offset 10).

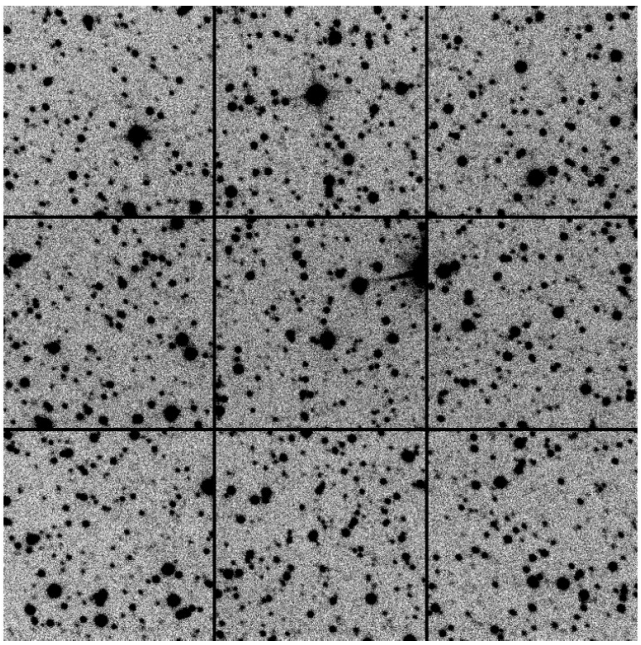

Figure 7. ASTAP aberration inspector for the V425 Cas field: a 3×3 grid of stellar cutouts sampling the corners, edges, and center of the frame, used to assess spatial variations of the PSF and field-dependent optical aberrations.

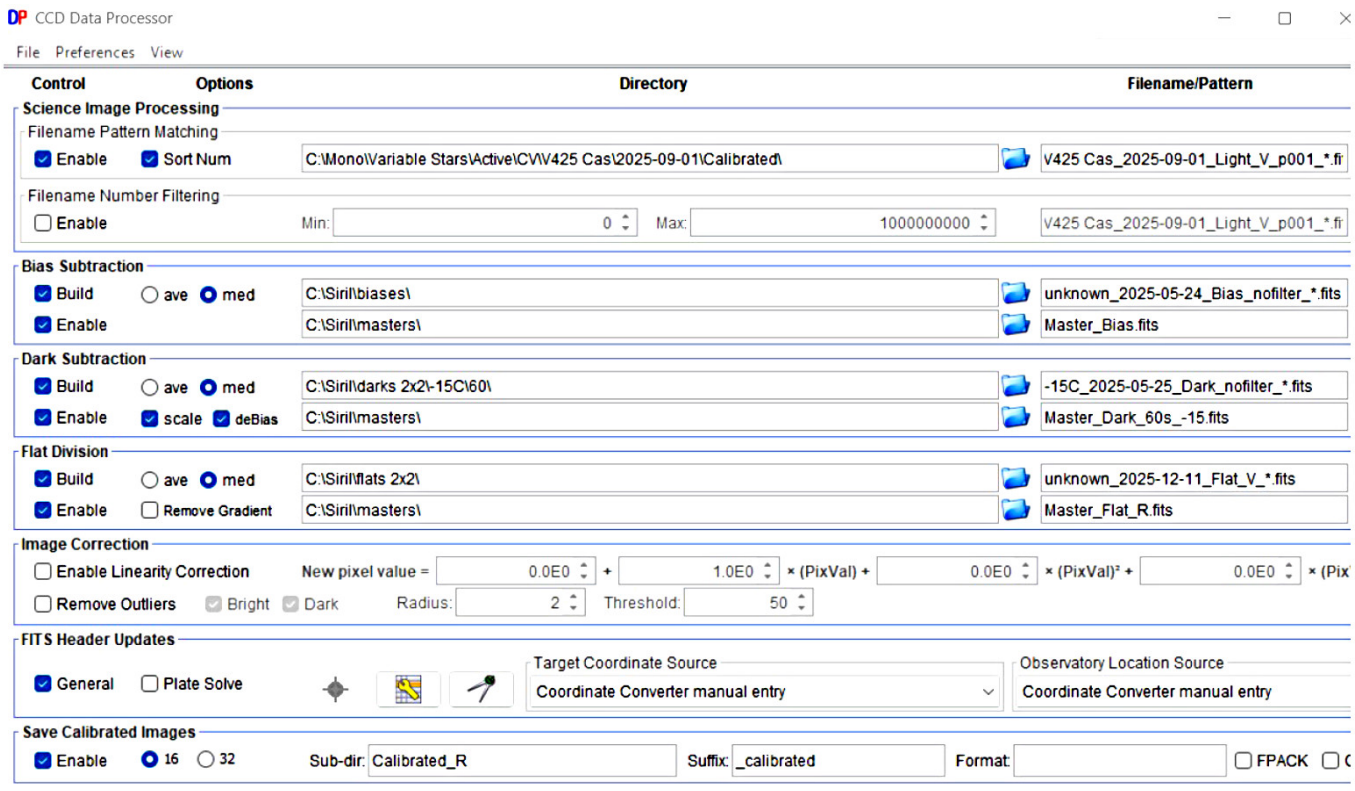

Figure 8. AstroImageJ Data Processor interface for building master calibration frames and calibration of science images.

2.5. Calibration strategy

The calibration of the science images followed standard CCD reduction procedures, including the acquisition of bias, dark, and flat-field frames, and was performed using AstroImageJ (Collins *et al.* 2017), as illustrated in Figure 8.

Bias frames were obtained with the telescope aperture closed, using an exposure time of 0 s. A total of 99 bias frames were acquired and later combined using the median method.

Dark frames were also taken with the telescope aperture closed, matching both the exposure time and the CCD temperature used during the scientific observations. Typically, the camera operated at –20° C, a temperature at which, according to the manufacturer's specifications, the thermal noise of the detector is negligible. If environmental conditions did not allow operation at this temperature, the camera was set to at least –15° C. For each of these operating temperatures, dedicated dark frames were obtained using the same exposure and temperature as those in the observations.

The enabled calibration options in the AstroImageJ CCD Data Processor are summarized in Table 4.

Flat fields (see Figure 9) were obtained immediately after sunset. The exposure time was adjusted so that the mean pixel value in each frame was maintained at ~30,000 ADU, well within the linear response range of the camera. At least seven flat-field frames were taken for each filter, and all calibration frames were stacked using median combining to remove cosmic rays and residual artifacts. AstroImageJ generates a normalized master flat by scaling individual frames to a common intensity level. This master flat is then applied to science images by division.

Table 4. AstroImageJ (AIJ) CCD Data Processor calibration options.

Step	*Enabled Options*
Bias subtraction	Build master bias; apply bias subtraction; combine method: median
Dark subtraction	Build master dark; apply dark subtraction; deBias; dark scaling; combine method: median
Flat division	Build master flat; apply flat-field correction; combine method: median

Figure 9. A master flat field obtained in the V filter, created from the median combination of multiple twilight flats.

3. Results

Data from the Meshtitsa Observatory are available through the AAVSO (Kloppenborg 2025) and are already being used in astronomical research. Exoplanet transit observations have likewise been incorporated into NASA's Exoplanet Watch[12] database. The following section presents several new results that demonstrate the capabilities of small telescopes such as the one at the Meshtitsa Observatory.

3.1. Superhumps of dwarf nova GOTO065054+593624

The dwarf nova GOTO065054+593624 (GOTO0650) was discovered on 4 October 2024 (Killestein *et al.* 2024), by the GOTO all-sky survey[13] and quickly identified by volunteers from the Kilonova Seekers[14]. Their rapid classification allowed immediate follow-up, revealing a WZ Sge type cataclysmic star with an 8.5-magnitude outburst (Killestein *et al.* 2025). The Meshtitsa Observatory joined the follow-up campaign and conducted observations over 26 nights, spanning 98 hours, across a two-month period, making it one of the sites that detected the first superhumps of the star during its outburst.

Among all observations, superhumps were identified in a total of six instances. The observations listed in Table 5, were processed using AstroImageJ. The periodogram at Figure 10 reveals the first detected superhumps for the GOTO0650, visible as periodic brightness modulation with an amplitude of 0.06 (M). Using the Generalized Lomb–Scargle (Zechmeister and Kürster 2009), the superhump period was determined to be $\approx 91 \pm 1$ min.

The superhump period is crucial for determining the mass ratio of the system's components (Kato and Osaki 2013). This is done through the *superhump period excess*,

$$\epsilon = \frac{P_{sh}}{P_{orb}} - 1 \qquad (1)$$

where P_{sh} is the measured superhump period and P_{orb} is the orbital period of the binary.

Typical superhump period excesses in WZ Sge systems range from 0.8% to 1.5%. Assuming GOTO0650 follows this trend, the orbital period can be tentatively constrained to lie in the 88–90 minute range, e.g. Killestein *et al.* (2025). However, applying this relation requires an independent measurement of the orbital period P_{orb}, typically obtained through radial velocity studies.

3.2. Transit of exoplanet TOI-2109b on 22 March 2024

TOI-2109b is an ultrahot Jupiter-like exoplanet discovered in 2021 by NASA's Transiting Exoplanet Survey Satellite (TESS)[15]. The planet orbits an F-type star located about 855 light years away. TOI-2109b possesses a mass of approximately 5.02 Jupiter masses and a radius about 1.35 Jupiter radii. Observations of newly discovered exoplanets are particularly valuable, as their ephemerides are still being refined.

A transit of TOI-2109b was observed from Meshtitsa Observatory on 22 March 2024. The observation was conducted using a photometric V filter with an exposure time of 60 seconds per frame. Over approximately 4 hours, a total of 215 frames were captured. Both the photometric measurements and the

Table 5. Photometric observations of GOTO0650 with superhump period determination.

Obs. Start UTC	*Obs. End UTC*	*Dur. (h)*	*Mean Mag. V*	*Mean Err. V*	*Ampl. Mag. V*	*Period*
10/20/2024 19:45	10/21/2024 2:39	6.9	14.220	0.011	0.055	0.06332
10/22/2024 19:18	10/23/2024 2:54	7.6	14.275	0.016	0.034	0.06293
10/23/2024 19:48	10/24/2024 2:42	6.9	14.352	0.013	0.032	0.06382
10/25/2024 19:38	10/26/2024 2:56	7.3	14.534	0.015	0.030	0.06327
10/26/2024 19:28	10/27/2024 2:22	6.9	14.639	0.015	0.025	0.06196
10/27/2024 19:49	10/28/2024 2:25	6.6	14.744	0.015	0.022	0.06334

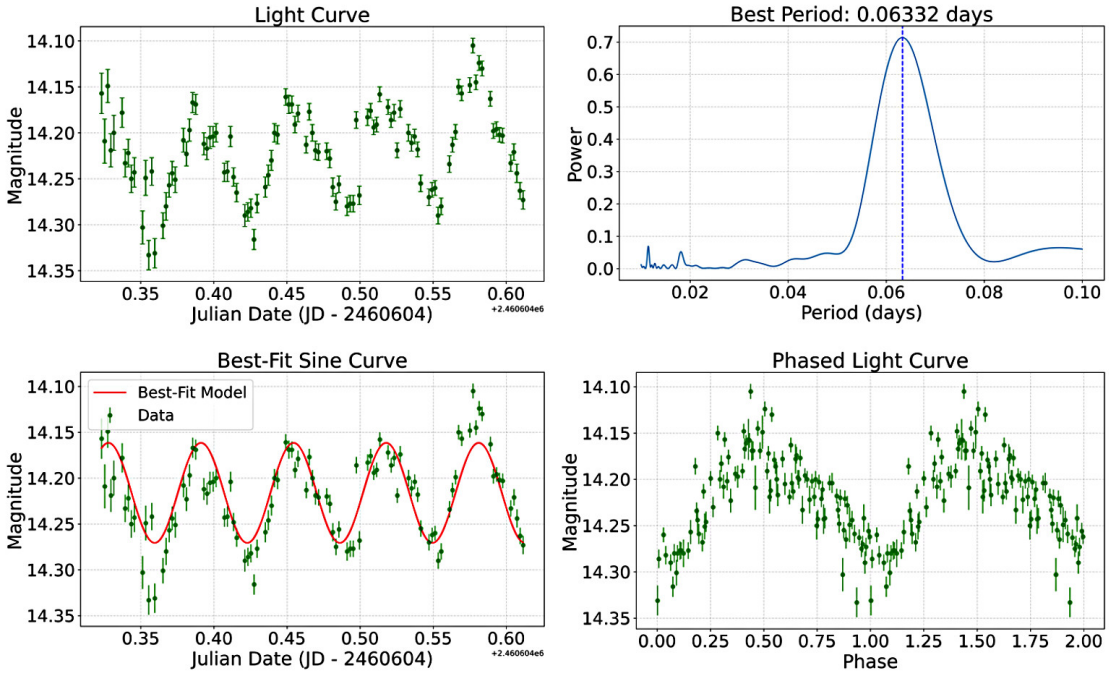

Figure 10. Periodogram and V-band light curve from the first observing night on Oct 20, 2024 on which superhumps of GOTO0650 were detected. The period derived with the Generalized Lomb–Scargle algorithm was used to compute the best-fitting sinusoid over the original photometric data.

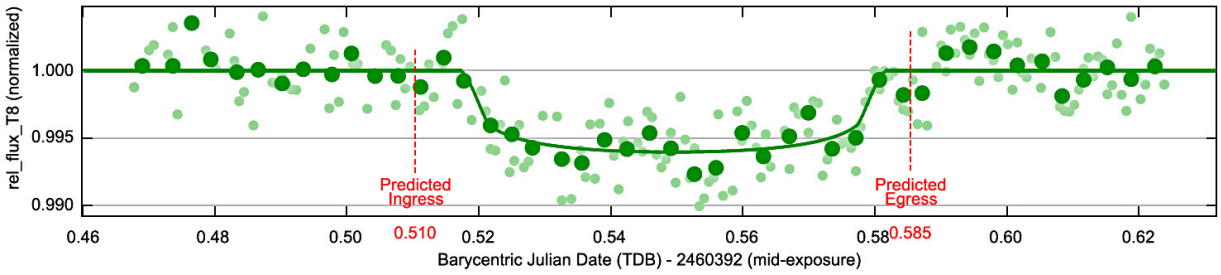

Figure 11. Relative flux light curve of TOI-2109b based on 215 V-band exposures taken on 22 March 2024. The data points represent the differential photometry of the target star using nearby comparison stars. The smooth model curve shows the best-fit transit profile calculated within AstroImageJ, based on the observed flux decrease during the planetary transit. The characteristic U-shape reflects the partial occultation of the stellar disk by the orbiting planet.

Table 6. Flares of AD Leo captured between 16 January and 2 May 2025 in B band (Johnson B filter) with a 30-seconds cadence.

Flare No.	*Flare Start JD*	*Flare End JD*	*Dur. (min)*	*Peak JD*	*Peak Mag.*	*δ Mag.*	*Energy in B (erg)*
1	2460695.39903	2460695.42996	45	2460695.40336	10.32	0.51	1.90e+32
2	2460710.32434	2460710.33953	22	2460710.32990	10.66	0.18	2.48e+31
3	2460712.39542	2460712.42106	37	2460712.40529	10.69	0.15	1.60e+31
4	2460721.37398	2460721.38063	10	2460721.37651	10.78	0.06	1.74e+30
5	2460727.39928	2460727.41245	19	2460727.40507	10.04	0.81	7.00e+31
6	2460727.41513	2460727.42673	17	2460727.41738	10.69	0.16	1.45e+31
7	2460729.45763	2460729.46819	15	2460729.46021	10.74	0.11	3.47e+31
8	2460729.51584	2460729.52411	12	2460729.51942	10.77	0.08	3.38e+30
9	2460732.31972	2460732.38421	93	2460732.32789	10.11	0.74	1.06e+33
10	2460732.38772	2460732.39952	17	2460732.39038	10.10	0.75	3.02e+32
11	2460739.31536	2460739.33539	29	2460739.32174	10.46	0.39	2.28e+32
12	2460739.33812	2460739.38395	66	2460739.34096	10.04	0.81	2.46e+32
13	2460739.46924	2460739.48108	17	2460739.47281	10.58	0.27	3.21e+31
14	2460756.27626	2460756.30324	39	2460756.27891	10.33	0.51	1.90e+32
15	2460773.27872	2460773.28845	14	2460773.28205	10.75	0.09	2.63e+31
16	2460773.31697	2460773.32446	11	2460773.31929	10.77	0.08	1.47e+31

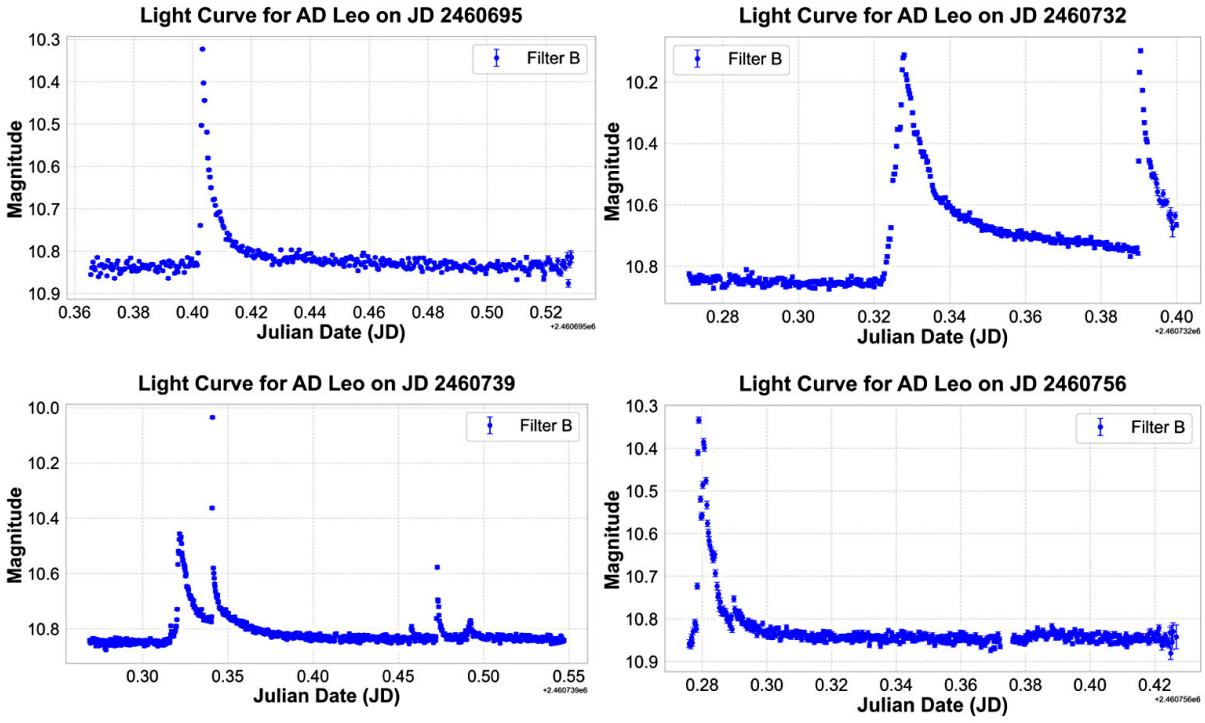

Figure 12. Light curves of several of the most characteristic AD Leo flares obtained at Meshtitsa Observatory in the B filter with a 30-second cadence.

transit model fit, shown in Figure 11, were derived using AIJ's built-in differential photometry and fitting tools.

The transit light curve of TOI-2109b obtained on 22 March 2024 was modeled using the fitting tools in AstroImageJ. The best-fit parameters are consistent with the published ephemerides, e.g. Wong *et al.* (2021).

The fitted planet-to-star radius ratio is $(R_p / R_*)^2 = 0.00511$, corresponding to a transit depth of 6.0 ppt. The total transit duration was measured as $t_{14} = 0.0646$ d ($01^h 33^m 01^s$). Assuming the stellar radius $R_* = 1.698\ R_\odot$, this corresponds to a planetary radius of $R_p = 1.18\ R_{Jup}$. The fit yields a transit geometry with an inclination of $i \approx 71°$.

The quality of the fit is reflected by the statistical indicators: the RMS of the residuals is 0.00207 in normalized flux (~2.1 ppt), and the reduced chi-square is $\chi^2 / \mathrm{dof} = 1.07$.

3.3. Flares of AD Leo captured between 16 January and 2 May 2025

AD Leo is a dM3.5e star, only about 5 pc from the Sun. Statistical analyses indicate that it produces energetic flares at a moderate rate and ranks among the most thoroughly studied flare stars in the solar neighborhood, e.g. Pettersen and Coleman (1981).

Table 6 lists 16 B-band flares of AD Leo observed with a 30-s cadence between 16 January and 2 May 2025. Energies were calculated by applying the standard time integration of the luminosity, widely formalized by flare-energy studies, e.g. Hunt-Walker *et al.* (2012). The software used in energy calculation is a custom in-house Python-based program developed specifically for this project. At present, it is not publicly released.

Representative AD Leo light curves in Figure 12 display the classic fast-rise-exponential-decay (FRED) flare profiles.

4. Conclusions

In this study, selected first results from observations conducted with the remote Meshtitsa Observatory were presented:

- V-band monitoring during the outburst of the dwarf nova GOTO065054 revealed the onset of superhumps and yielded a period of 91 ± 1 min.
- A transit observation of TOI-2109b revealed a duration of 0.0646 d with a depth of 6.0 ppt, aligning with predicted values, and yielded key statistics on which the planetary radius estimate rests.
- Several high-cadence B-band flares on AD Leo were presented.

These results show that observations from small, non-professional observatories achieve sufficient precision for use in professional studies. Their capacity for frequent, targeted monitoring makes them an indispensable part of global astronomical networks, especially for tracking dynamic or unpredictable objects that larger surveys may miss. Beyond the individual results, this work affirms the strategic role of citizen-science observatories in modern time-domain astronomy. Currently, Meshtitsa Observatory continues to conduct regular observations and participate in international campaigns.

5. Acknowledgements

The author gratefully acknowledges the anonymous referees for their thoughtful critiques and recommendations, which helped refine the article. The equipment for the Meshtitsa Observatory was provided through donations from Scorpion Shipping Ltd.[16] and the Institute for Advanced Physical Studies, Sofia, Bulgaria[17]. Sincere gratitude is extended to Sean Curry, Bob Buchheim, Gary Hawkins, and Thomas Smith for providing the custom Python-based software PhotoStats, which was instrumental in performing the calculations of flare energy presented in this work.

References

AAVSO. 2022, AAVSO Guide to CCD/CMOS Photometry (https://www.aavso.org/ccd-camera-photometry-guide).

AAVSO. 2014, AAVSO Transform Generator (https://www.aavso.org/tg).

Baader Planetarium. 2026, Baader Planetarium website: (https://www.baader-planetarium.com/).

Benz, A. O., and Güdel, M. 2010, *Annu. Rev. Astron. Astrophys.*, **48**, 241.

Collins, K. A., Kielkopf, J. F., Stassun, K. G., and Hessman, F. V. 2017, *Astron. J.*, **153**, 77.

Fowler, M. J. F., Sienkiewicz, F. F., Zellem, R. T., and Dussault, M. E. 2021, *J. British Astron. Assoc.*, **131**, 359.

Hunt-Walker, N. M., Hilton, E. J., Kowalski, A. F., Hawley, S. L., and Matthews, J. M. 2012, *Publ. Astron. Soc. Pacific*, **124**, 545.

Kato, T., and Osaki, Y. 2013, *Publ. Astron. Soc. Japan*, **65**, 115.

Killestein, T. L., *et al.* 2025, *Astron. Astrophys.*, **699A**, 8.

Killestein, T., *et al.* 2024, *Astron. Telegram*, No. 16842, 1.

Kloppenborg, B. 2025, variable star observations from the AAVSO International Database (https://apps.aavso.org/v2/data/search/photometry).

NASA. 2026, Exoplanet Watch (https://science.nasa.gov/citizen-science/exoplanet-watch).

National Research Council (NRC). 2015, *Optimizing the U.S. Ground-Based Optical and Infrared Astronomy System*, The National Academies Press, Washington, DC, 26.

Pettersen, B. R., and Coleman, L. A. 1981, *Astrophys. J.*, **251**, 571.

Suzhou ZWO Co., Ltd. 2026, ZWO Astro ASI533 Pro Series camera (https://www.zwoastro.com/product/asi533-pro-series).

Wong, I., *et al.* 2021, *Astron. J.*, **162**, 256.

Zechmeister, M., and Kürster, M. 2009, *Astron. Astrophys.*, **496**, 577.

Zellem, R. T., *et al.* 2020, *Publ. Astron. Soc. Pacific*, **132**, 054401.

Notes

[1] https://orcid.org/0009-0002-1484-7029
[2] Sky-Watcher Telescope N 250/1200: https://skywatcher.com/product/bkp-250-ds/
[3] Sky-Watcher Telescope EQ6-R Pro: https://skywatcher.com/product/eq6r-pro/
[4] TS Optics Guidescope AC 80/600: https://www.teleskop-express.de/en/telescopes-4/achromatic-refractor-54/ts-opticsguiding-scope-80-600-mm-with-adjustable-tube-rings-8797/
[5] ZWO Astro ASI290MC camera: https://www.zwoastro.com/product-category/cameras/
[6] INDIGO platform: https://www.indigo-astronomy.org/
[7] CloudWatcher: https://lunaticoastro.com/aag-cloud-watcher/
[8] Baader UBVR Bessel filter set: https://www.baader-planetarium.com/en/baader-ubvri-bessel-filter-setphotometric.html/
[9] ZWO Astro ASI 533 MM Pro: https://www.zwoastro.com/product/asi533-pro-series/
[10] ASTAP astrometric software: https://www.hnsky.org/astap.htm/
[11] Lunatico Astronomia CloudWatcher: https://www.lunaticoastro.com
[12] NASA Exoplanet Watch: https://exoplanets.nasa.gov/exoplanet-watch/about-exoplanet-watch/overview/
[13] GOTO all sky survey: https://goto-observatory.org/
[14] Kilonova Seekers: https://www.zooniverse.org/projects/tkillestein/kilonova-seekers/
[15] NASA Transiting Exoplanet Survey: https://tess.mit.edu/
[16] Scorpion Shipping Ltd.: https://scorpion-shipping.net/
[17] Institute for Advanced Physical Studies: https://iaps.institute/